Supplementary files for

Postnatal depression-associated breastmilk microRNAs in small extracellular vesicles: Intergenerational impacts on offspring neurological development

This PDF file includes:

Supplementary Figure 1 to 18.

Supplementary Table 1 to 3.

Supplementary Figures

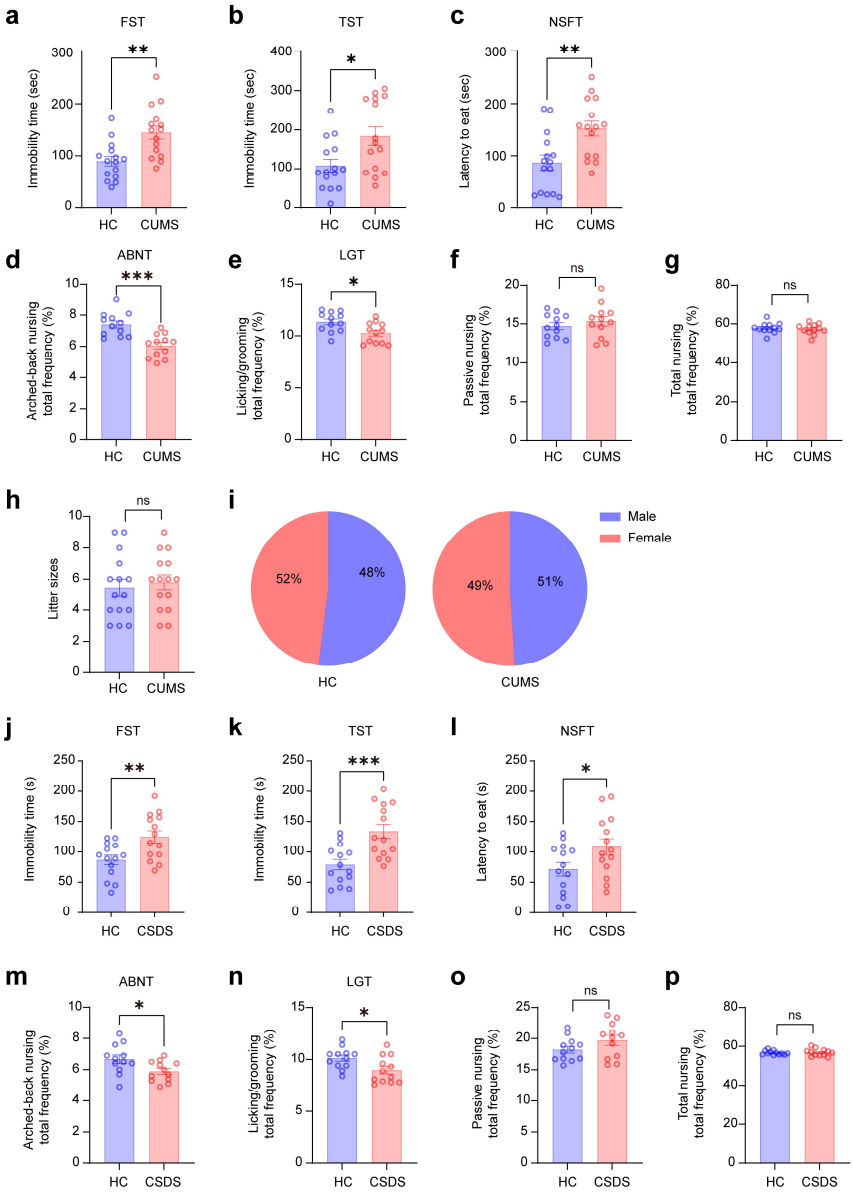

Supplementary Figure 1. Depression-like phenotypes in female C57BL/6 mice induced by CUMS and CSDS paradigms a, Immobility time in the FST for HC and CUMS-induced dams (n = 15 per group). **b,** Immobility time in the TST for HC and CUMS-induced dams (n = 15 per group). **c,** Latency to eat in the NSFT for HC and CUMS-induced dams (n = 15 per group). **d-e,** Effects of CUMS on maternal arched-back nursing **(d)** and licking/grooming **(e)** behaviors, recorded from postpartum days 3-15 in HC and CUMS-induced dams. Data are presented as the percentage frequency of each behavior relative to total observations over the monitoring period (n = 12 per group). **f-g,** Effects of CUMS on passive nursing **(f)** and total nursing duration **(g)** in HC and CUMS-induced dams, observed from postpartum days 3-15 (n = 12 per group). **h,** Bar graph showing the litter size for HC and CUMS-induced dams. **i,** Pie chart illustrating the distribution of offspring sex ratio in HC and CUMS-induced dams. **j,** Immobility time in the FST for HC and CSDS-induced dams (n = 14 per group). **k,** Immobility time in the TST for HC and CSDS-induced dams (n = 14

per group). **l,** Latency to eat in the NSFT for HC and CSDS-induced dams (n = 14 per group). **m-n,** Effects of CSDS on maternal arched-back nursing **(m)** and licking/grooming **(n)** behaviors, recorded from postpartum days 3-15 in HC and CSDS-induced dams (n = 12 per group). **o-p,** Effects of CSDS on passive nursing **(o)** and total nursing duration **(p)** in HC and CSDS-induced dams, observed from postpartum days 3-15 (n = 12 per group). Data are presented as mean ± SEM. Statistical analysis was performed using two-sided unpaired t-test (**a-h** and **j-p**). *$p < 0.05$; **$p < 0.01$; ***$p < 0.001$; ns, not significant.

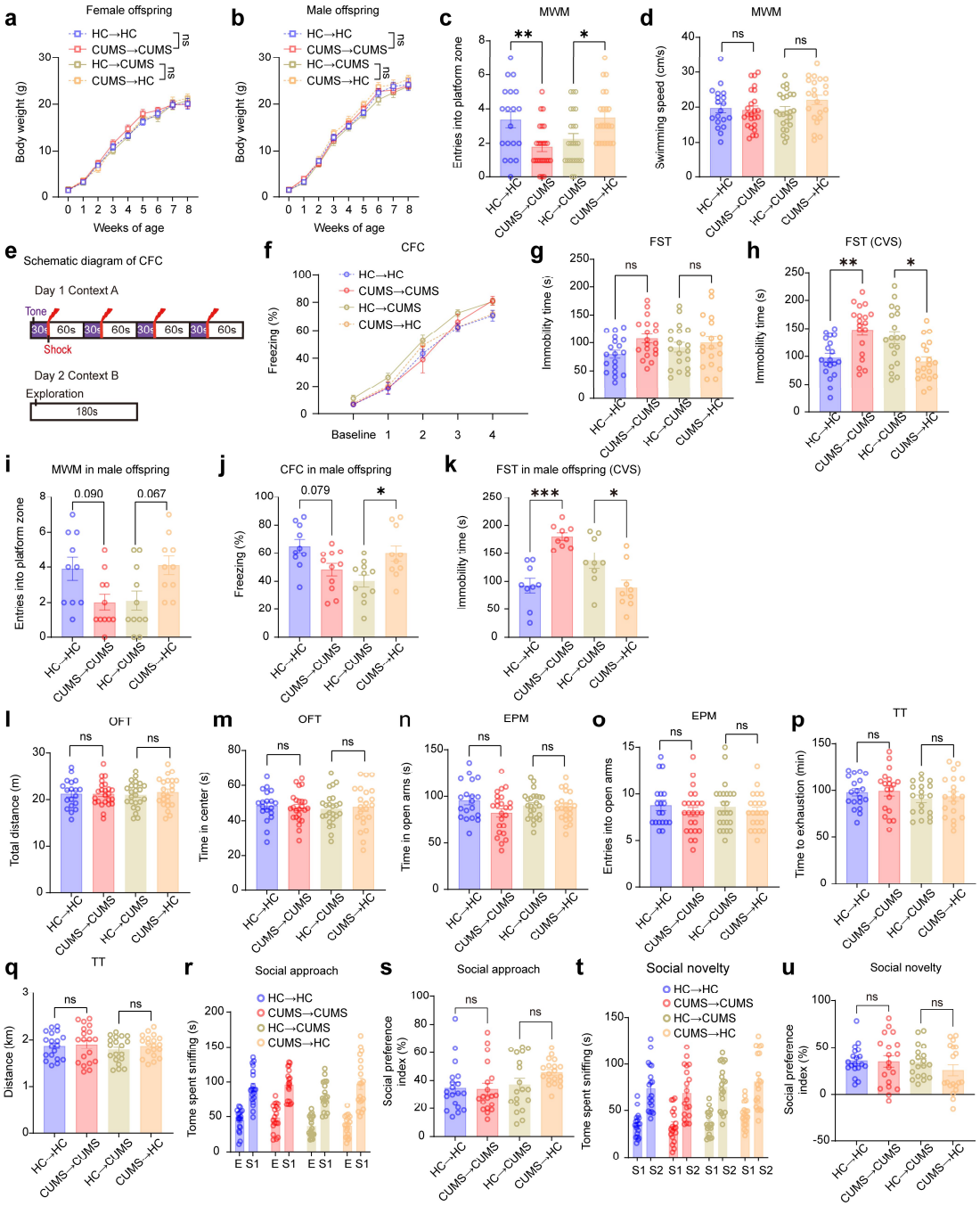

Supplementary Figure 2. Behavioral performance among offspring cross-fostered by HC and CUMS-induced dams. a-b, Body weight changes in female **(a)** and male **(b)** offspring (n = 9 for male groups, n = 10 for female groups). **c,** Number of entries into the platform zone in the probe trial of the MWM test (n = 19 for HC→HC; n = 24 for CUMS→CUMS and HC→CUMS; n = 22 for CUMS→HC). **d,** Total swimming activity in the MWM test (n = 19 for HC→HC; n = 24 for CUMS→CUMS and HC→CUMS; n = 22 for CUMS→HC). **e,** Experimental scheme of the CFC test. **f,** Freezing percentage in the training phase of the CFC test (n = 19 for HC→HC; n = 24 for CUMS→CUMS and HC→CUMS; n = 22 for CUMS→HC). **g,** Immobility time in the FST under baseline conditions (n = 19 per group). **h,** Immobility time in the FST after exposure to CVS (n = 19 per group). **i,** Number of entries into the platform zone in the probe trial of the MWM test among groups of male offspring (n = 10 for HC→HC and CUMS→HC, n = 11 for CUMS→CUMS and

HC→CUMS). **j,** Freezing percentage in the conditioning session of the CFC test among groups of male offspring (n = 10 for HC→HC and CUMS→HC, n = 11 for CUMS→CUMS and HC→CUMS). **k,** Immobility time in the FST after exposure to CVS among groups of male offspring (n = 10 for HC→HC and CUMS→HC, n = 11 for CUMS→CUMS and HC→CUMS). **l-m,** Total distance traveled **(l)** and time spent in the center **(m)** in the OFT (n = 19 for HC-HC; n = 24 for CUMS-CUMS and CUMS-HC; n = 22 for HC-CUMS). **n-o,** Time spent in open arms **(n)** and open arm entries **(o)** in the EPM test (n = 19 for HC-HC; n = 24 for CUMS-CUMS and CUMS-HC; n = 22 for HC-CUMS). **p-q,** Running time to exhaustion **(p)** and the maximum distance traveled **(q)** in the TT (n = 19 per group). **r,** Total time spent sniffing the empty cage (E) and the cage with Stranger Mouse 1 (S1) (n = 19 per group). **s,** Social approach preference index calculated during the social approach stage (n = 19 per group). **t,** Total time spent sniffing Stranger Mouse 1 (S1) and Stranger Mouse 2 (S2) (n = 19 per group). **u,** Social novelty preference index calculated during the social novelty stage (n = 19 per group). Data are presented as mean ± SEM. Statistical analysis was performed using one-way ANOVA followed by Bonferroni's multiple comparisons test (**c, d, g-q, s,** and **u**), or two-way ANOVA followed by Bonferroni's multiple comparisons test (**a** and **b**). *$p < 0.05$; **$p < 0.01$; ***$p < 0.001$; ns, not significant.

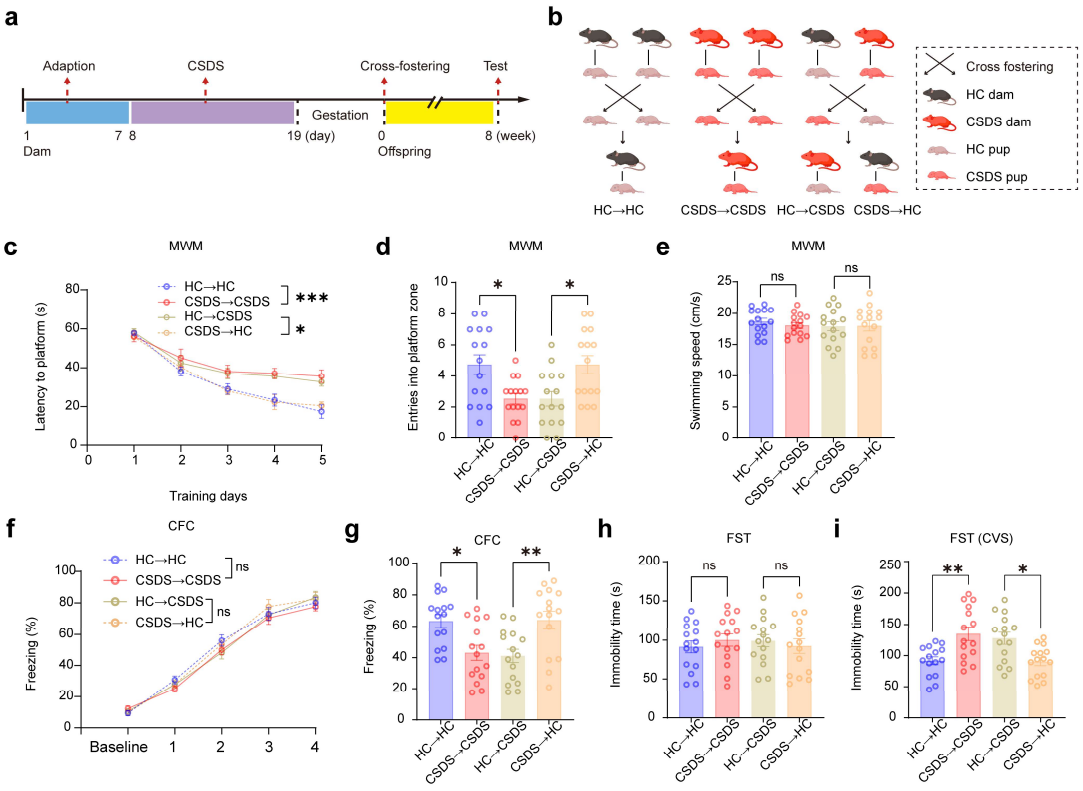

Supplementary Figure 3. Behavioral performance among offspring cross-fostered by HC and CSDS-induced dams. a, Schematic of the experimental design. Female C57BL/6J mice were exposed to CSDS paradigms to induce PND. Their offspring were cross-fostered at birth to control for genetic effects and underwent behavioral and neurobiological assessments at P56. **b,** Cross-fostering scheme. Immediately after birth, offspring from CSDS or HC dams were cross-fostered by either CSDS or HC dams, generating four groups (HC→HC, CSDS→CSDS, HC→CSDS, and CSDS→HC) designated as birth mother→foster mother. **c,** Latency to locate the hidden platform in the training trial of the MWM test (n = 15 per group). **d,** Number of entries into the platform zone in the probe trial of the MWM test (n = 15 per group). **e,** Total swimming activity in the MWM test (n = 15 per group). **f,** Freezing percentage in the training phase of the CFC test (n = 15 per group). **g,** Freezing percentage in the conditioning session of the CFC test (n = 15 per group). **h,** Immobility time in the FST under baseline conditions (n = 15 per group). **i,** Immobility time in the FST after exposure to CVS (n = 15 per group). Data are presented as mean ± SEM. Statistical analysis was performed using one-way ANOVA followed by Bonferroni's multiple comparisons test (**d, e, g, h,** and **i)**, or two-way ANOVA followed by Bonferroni's multiple comparisons test (**c** and **f**). *$p < 0.05$; **$p < 0.01$; ns, not significant.

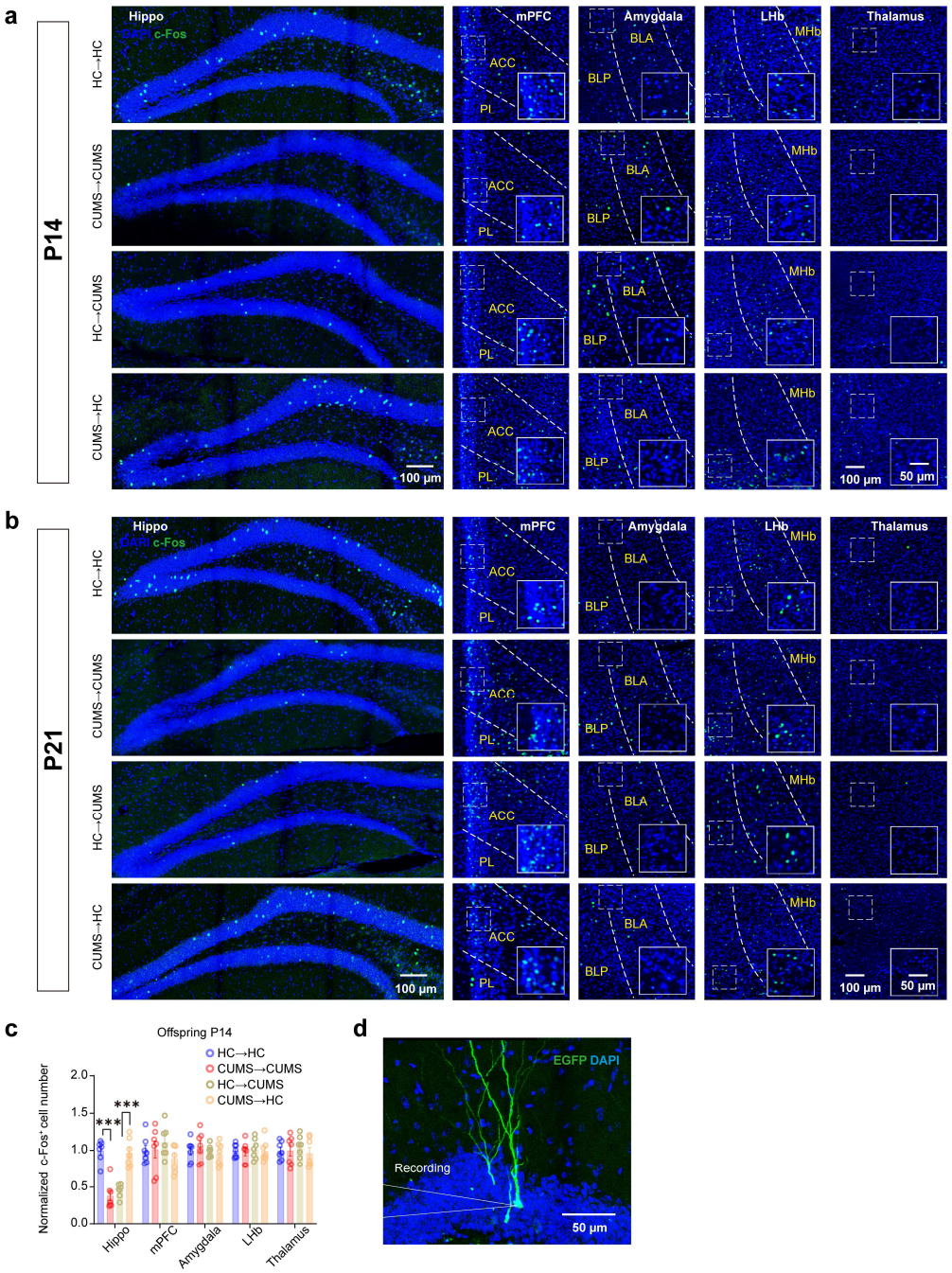

Supplementary Figure 4. Mapping of c-Fos$^+$ neuronal activation across brain regions in cross-fostered offspring. a-b, Representative images of c-Fos immunostaining in various brain regions related to cognition and emotion, including the hippocampus, medial prefrontal cortex (mPFC), amygdala, lateral habenula (LHb), and thalamus, in HC-CUMS and CUMS-HC offspring at P14 **(a)** and P21 **(b)**. Scale bars: 100 μm (overview), 50 μm (inset). **c,** Quantification of c-Fos$^+$ cells across the indicated brain regions at P14 (n = 7 per group). **d,** Representative images of recorded newborn neurons, identified and confirmed by EGFP$^+$ immunostaining signals (green) following RV-EGFP injection. Scale bars: 50 μm. Data are presented as mean ± SEM. Statistical analysis was performed using one-way ANOVA followed by Bonferroni's multiple comparisons test (C). ***$p < 0.001$.

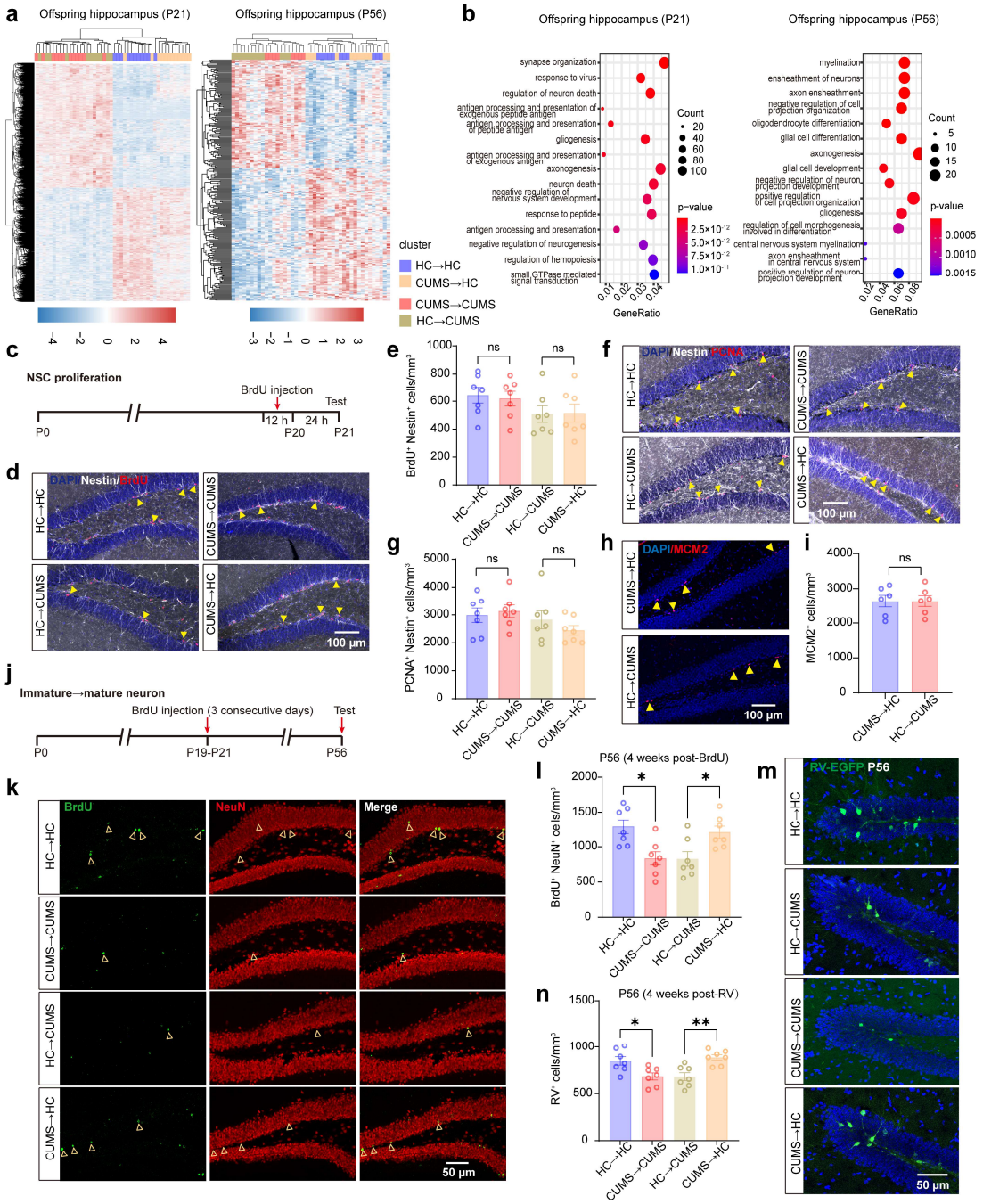

Supplementary Figure 5. Assessment of NSC proliferation and newborn neuron maturation in cross-fostered offspring. a, Heatmap illustrating the differentially expressed hippocampal genes among the four offspring groups at P21 (left) and P56 (right) (n = 11 for HC→HC; n = 8 for CUMS→CUMS; n = 12 for HC→CUMS and CUMS→HC). **b,** GO enrichment analysis of the DEGs comparing the two main groups (HC→HC + CUMS→HC versus CUMS→CUMS + HC→CUMS) at P21 (left) and P56 (right). Top 15 enriched GO terms in biological processes and molecular functions are shown based on adjusted p-values. **c,** Experimental scheme for assessing NSC proliferation. Cross-fostered offspring received BrdU injections at P20 and were analyzed 24 hours later. **d,** Representative images of Nestin and BrdU co-staining in the DG. Arrowheads indicate double-positive cells. Scale bars: 100 μm. **e,** Quantification of $Nestin^{+}BrdU^{+}$ cells in the DG (n = 7 mice per group). **f,** Representative images of Nestin and PCNA co-staining in the DG.

Arrowheads indicate double-positive cells. Scale bars: 100 μm. **g,** Quantification of $Nestin^+PCNA^+$ cells in the DG (n = 7 mice per group). **h,** Representative images of MCM2 staining with DAPI in the DG. Arrowheads indicate colocalization of MCM2 with DAPI. Scale bars: 100 μm. **I,** Quantification of $MCM2^+$ cells in the DG (n = 6 mice per group). **j,** Experimental scheme for assessing newborn neuron maturation. BrdU was administered on three consecutive days (P19-P21) to label newborn neurons in mice, with neuronal maturation analysis conducted at P56. **k,** Representative images of BrdU and NeuN co-staining in the DG. Arrowheads indicate co-localization of BrdU and NeuN. Scale bars: 50 μm. **l,** Quantification of $BrdU^+$ cells co-expressing NeuN (n = 7 per group). **m,** Representative images of RV-EGFP-labeled newborn neurons in the DG. **n,** Quantification of $RV\text{-}EGFP^+$ cells in the DG at P56 (n = 7 mice per group). Data are presented as mean ± SEM. Statistical analysis was performed using one-way ANOVA followed by Bonferroni's multiple comparisons test (**e, g, l,** and **n**), or two-sided unpaired t-test (**i**). *$p < 0.05$; **$p < 0.01$; ns, not significant.

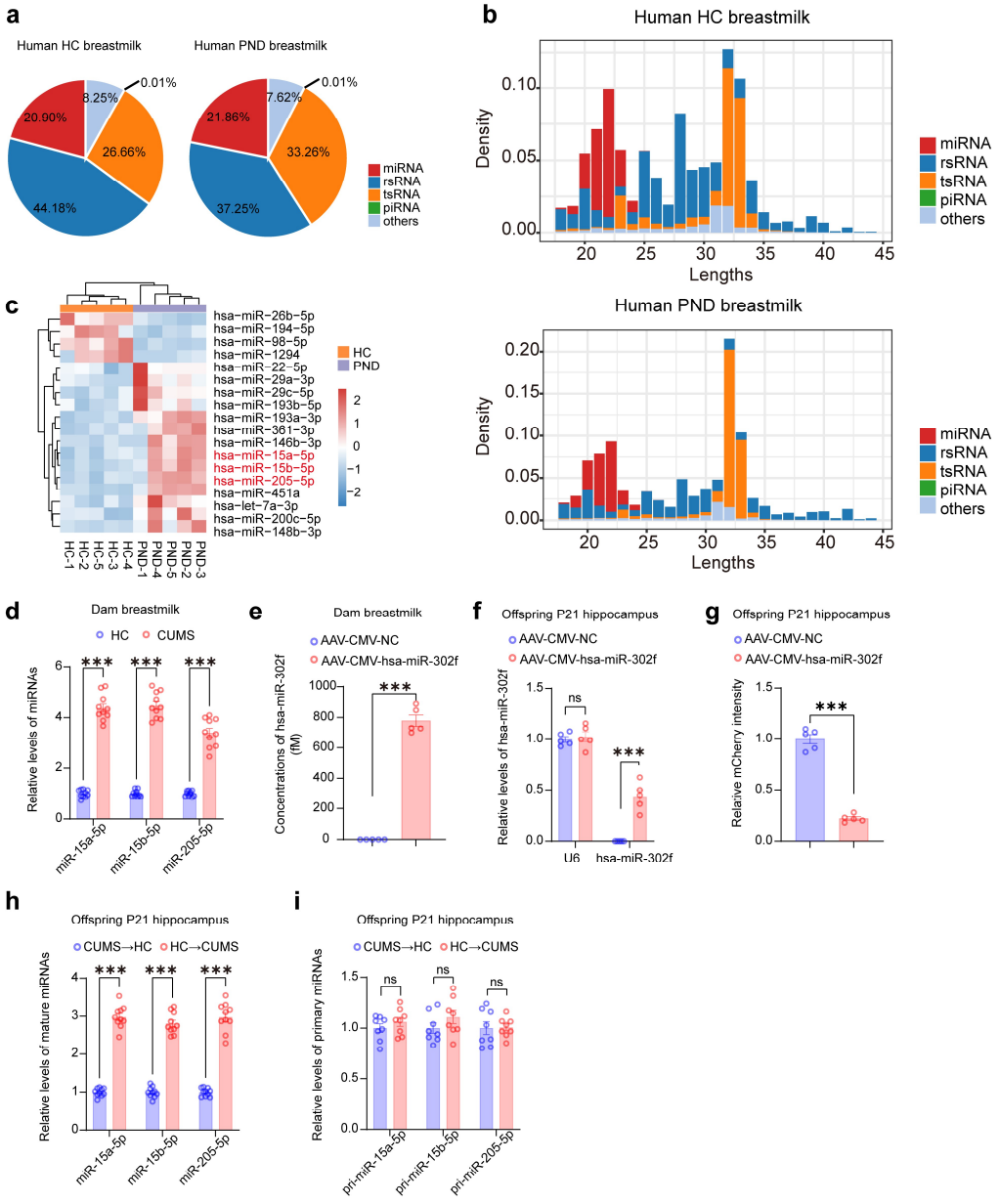

Supplementary Figure 6. sRNA profiling of breastmilk from PND patients and tracking of breastmilk miRNA delivery to offspring hippocampus. a, Pie chart showing the proportion of different sRNA types (miRNA, rsRNA, tsRNA, and piRNA) in total sRNAs from breastmilk of PND patients and HC mothers. **b,** Length distribution and composition of sRNAs in breastmilk, showing characteristic peaks for miRNAs (20-23 nt) and broader distributions for tsRNAs (23-34 nt) and rsRNAs (18-42 nt). **c,** Heatmap illustrating the differentially expressed breastmilk miRNAs (|fold change| > 2 and P < 0.05) between PND patients and HC mothers (n = 5 per group). **d,** Quantitative RT-PCR analysis of miR-15a-5p, miR-15b-5p, and miR-205-5p levels in breastmilk from CUMS-induced dams versus HC dams (n = 10 per group).**e,** Quantitative RT-PCR analysis of hsa_miR-302f levels in breastmilk after intramammary injection of AAV-CMV-hsa_miR-302f or AAV-CMV-NC (n = 5 per group). **f,** Quantitative RT-PCR analysis of hsa_miR-302f levels in offspring hippocampus after nursing by AAV-CMV-hsa_miR-302f- or AAV-CMV-NC-injected dams (n = 5 per group). U6 snRNA was used as an internal control. **g,** Quantification of mCherry

fluorescence intensity in offspring hippocampus after nursing by AAV-CMV-hsa_miR-302f- or AAV-CMV-NC-injected dams (n = 5 mice per group). **h,** Quantitative RT-PCR analysis of mature miR-15a-5p, miR-15b-5p, and miR-205-5p levels in hippocampus of HC→CUMS offspring versus CUMS→HC offspring (n = 10 per group). **i,** Quantitative RT-PCR analysis of pri-miR-15a-5p, pri-miR-15b-5p, and pri-miR-205-5p levels in hippocampus of HC→CUMS offspring versus CUMS→HC offspring (n = 8 per group). Data are presented as mean ± SEM. Statistical analysis was performed using two-sided unpaired t-test (**d-h** and **i**). ***$p < 0.001$; ns, not significant.

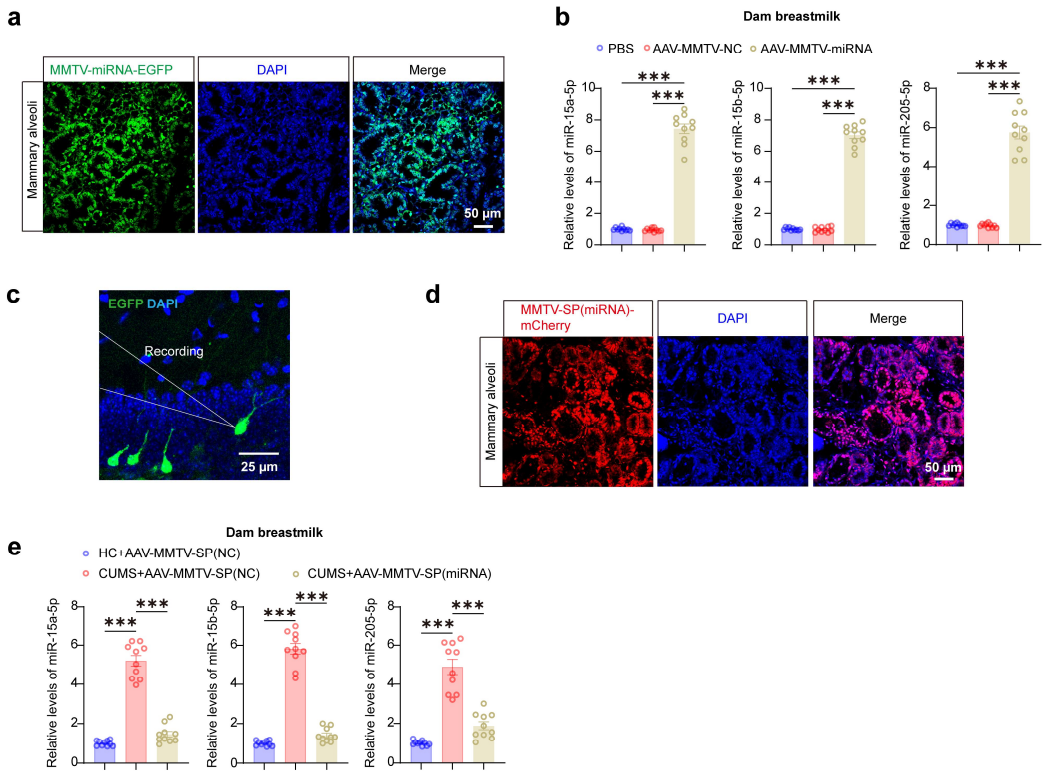

Supplementary Figure 7. Modulation of breastmilk miRNA levels via intraductal injection of AAV-MMTV-miRNA or AAV-MMTV-SP(miRNA) into mammary glands. a, Representative images of MMTV-miRNA-EGFP infections of mammary alveolar epithelial cells in the mammary gland. Scale bars: 50 μm. **b,** Quantitative RT-PCR analysis of miR-15a-5p, miR-15b-5p, and miR-205-5p levels in breastmilk from HC dams injected with PBS, AAV-MMTV-NC, or AAV-MMTV-miRNA (n = 10 per group). **c,** Representative image of recorded newborn neurons, identified and confirmed by $EGFP^{+}$ immunostaining signals (green) following RV-EGFP injection. Scale bars: 25 μm. **d,** Representative images of MMTV-SP(miRNA)-mCherry infections of mammary alveolar epithelial cells in the mammary gland. Scale bars: 50 μm. **e,** Quantitative RT-PCR analysis of miR-15a-5p, miR-15b-5p, and miR-205-5p levels in breastmilk from CUMS dams injected with AAV-MMTV-SP(miRNA) versus HC and CUMS dams injected with AAV-MMTV-SP(NC) (n = 10 mice per group). Data are presented as mean ± SEM. Statistical analysis was performed using one-way ANOVA followed by Bonferroni's multiple comparisons test (**a** and **c**). *$p < 0.05$; **$p < 0.01$; ***$p < 0.001$; ns, not significant.

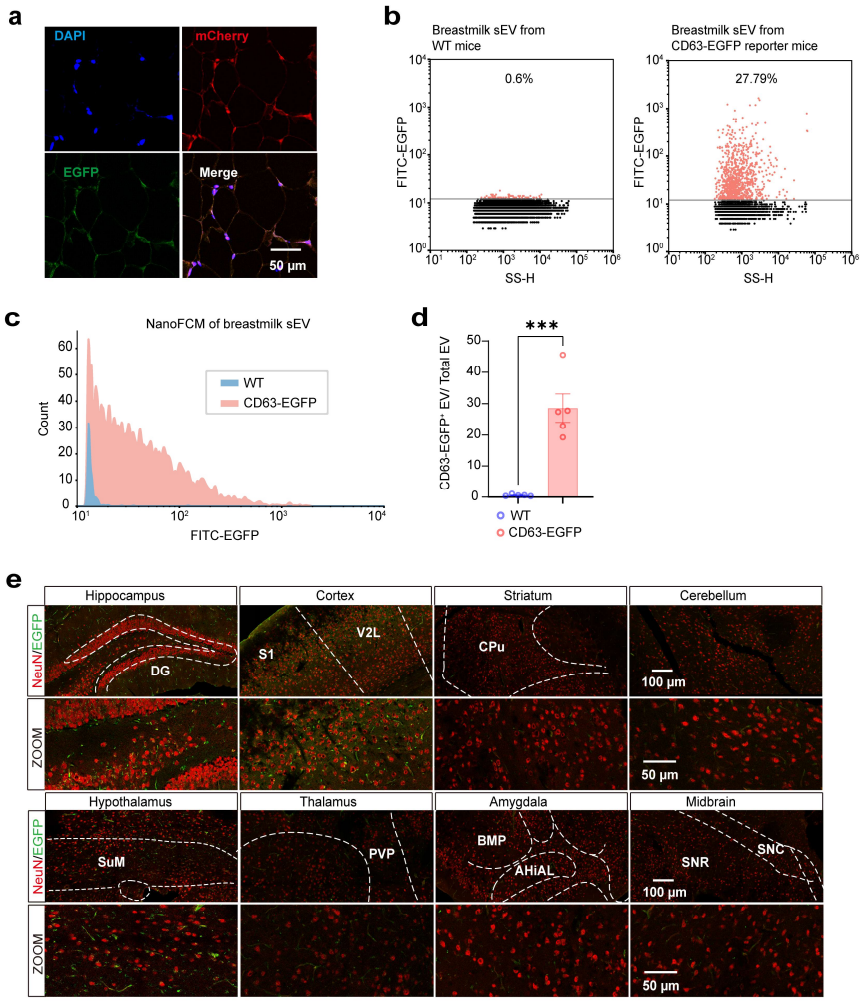

Supplementary Figure 8. ***In vivo*** **tracking of fluorescently labeled breastmilk sEVs delivered to the hippocampal DG of offspring.** Rosa26-CD63^{Flag}EGFP-mCherry knock-in mice were crossed with CAG-Cre mice to generate reporter offspring that systemically express the CD63^{Flag}EGFP-mCherry reporter gene, enabling the engineering and fluorescent tagging of sEVs with EGFP. When neonatal pups were fostered by these reporter dams, EGFP fluorescence was detected in multiple brain regions of the pups. **a,** Representative confocal images showing mCherry (red), EGFP (green), and DAPI (blue) fluorescence in the mammary tissues of female reporter mice expressing CD63^{Flag}EGFP-mCherry. Scale bars: 50 µm. **b-d,** NanoFCM analysis of EGFP^{+} sEVs isolated from the breastmilk of female wild-type (WT) and reporter mice. **(b)** Bivariate dot plot of EGFP versus side scatter for sEVs. **(c)** Histogram representing EGFP^{+} sEV populations. **(d)** Proportion of EGFP^{+} sEVs among total sEVs in WT versus reporter mice (n = 5 per group). **e,** Representative confocal images showing EGFP fluorescence (green) and NeuN immunostaining (red) in various brain regions of offspring nursed by female reporter mice. Scale bars: 100 µm (overview), 50 µm (zoom). Data are presented as mean ± SEM. Statistical analysis was performed using two-sided unpaired t-test (**d**). ***$p < 0.001$.

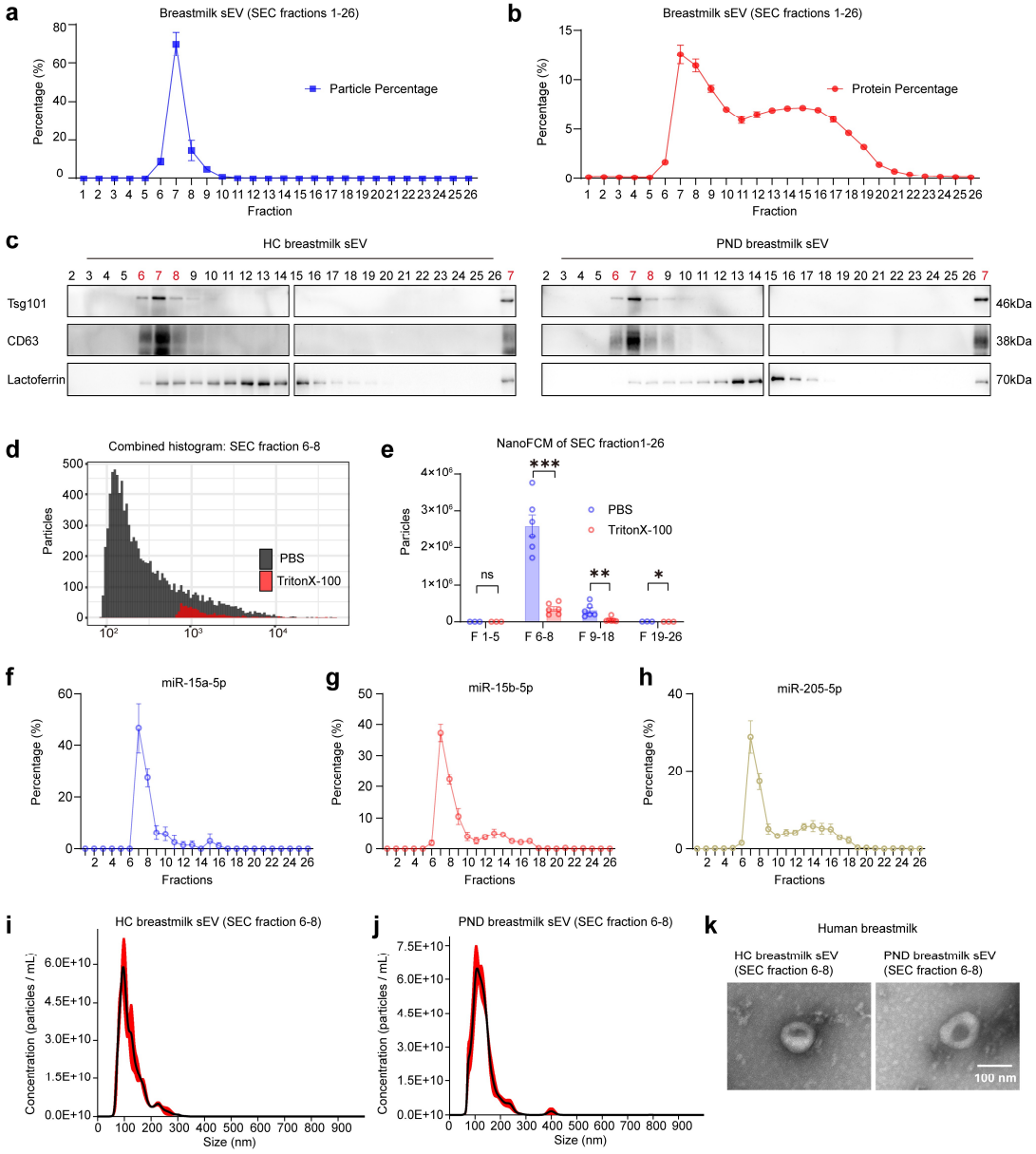

Supplementary Figure 9. Characterization of human breastmilk sEVs purified by differential ultracentrifugation combined with size-exclusion chromatography (dUC-SEC). Human breastmilk samples were processed by dUC to obtain a crude sEV pellet, which was further purified using SEC to generate 26 fractions. These fractions were subsequently analyzed to characterize the sEV components. **a-b,** Representative profiles showing the percentage distribution of particles **(a)** and proteins **(b)** across the SEC fractions. Particle concentration was determined by NTA, and protein concentration was measured using a BCA assay (n = 3 per group). **c,** Western blot analysis of sEV markers (TSG101 and CD63) and the breastmilk whey protein lactoferrin across the SEC fractions. **d-e,** The 26 SEC fractions were categorized into four groups based on particle and protein content: F1–5 (low particle, low protein), F6–8 (high particle, low protein), F9–18 (low particle, high protein), and F19–26 (low particle, low protein). These groups were analyzed by NanoFCM, and particle counts were evaluated before and after Triton X-100 treatment. Representative NanoFCM images **(d)** and quantitative particle counts **(e)** are shown (n = 6 for F6–8 and F9–18; n

= 3 for F1–5 and F19–26). **f-h,** Quantitative RT-PCR analysis of miR-15a-5p, miR-15b-5p, and miR-205-5p levels in each fraction, along with the percentage distribution of each miRNA (n = 3). **i-j,** Size distribution and concentration of sEVs (SEC fractions 6–8) isolated from breastmilk of PND patients and HC mothers, as measured by NTA. **k,** Representative TEM images of sEVs (SEC fractions 6–8) isolated from breastmilk of PND patients and HC mothers. Scale bars: 100 nm. Data are presented as mean ± SEM. Statistical analysis was performed using two-sided unpaired t-test (**e**). *$p < 0.05$; **$p < 0.01$; ***$p < 0.001$; ns, not significant.

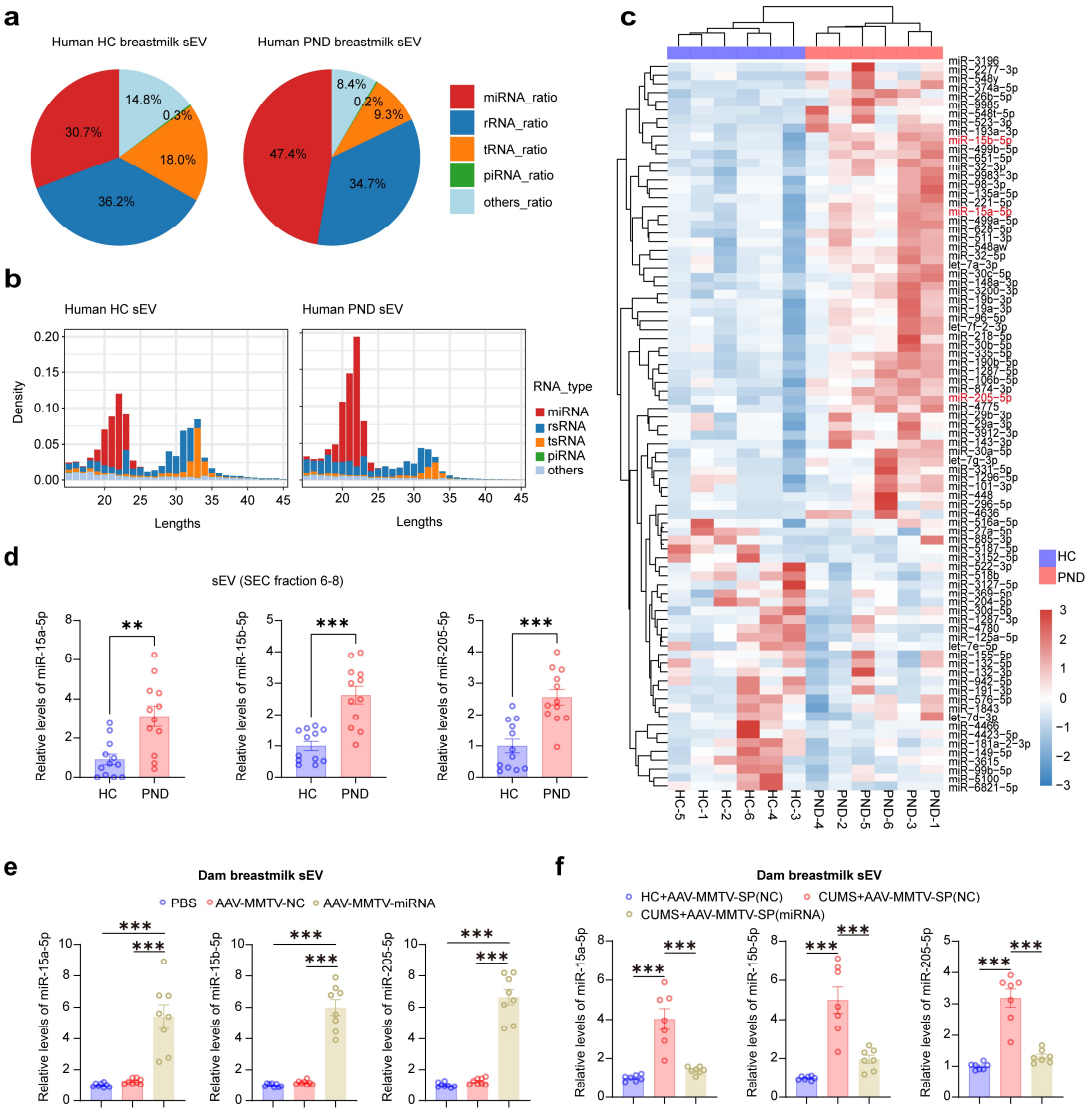

Supplementary Figure 10. sRNA profiling and quantitative RT-PCR analysis of breastmilk sEVs from PND patients and HC mothers. a, Pie chart showing the proportion of different sRNA types (miRNA, rsRNA, tsRNA, and piRNA) in total sRNAs from breastmilk sEVs of PND patients and HC mothers. **b,** Length distribution and composition of sRNAs in breastmilk sEVs, showing characteristic peaks for miRNAs (20-23 nt) and broader distributions for tsRNAs and rsRNAs. **c,** Heatmap illustrating the differentially expressed miRNAs in breastmilk sEVs from PND patients and HC mothers (n = 6 per group). **d,** Quantitative RT-PCR analysis of miR-15a-5p, miR-15b-5p, and miR-205-5p levels in breastmilk sEVs from PND patients versus HC mothers (n = 12 per group). **e,** Quantitative RT-PCR analysis of miR-15a-5p, miR-15b-5p, and miR-205-5p levels in breastmilk sEVs from HC dams injected with PBS, AAV-MMTV-NC, or AAV-MMTV-miRNA (n = 8 per group). **f,** Quantitative RT-PCR analysis of miR-15a-5p, miR-15b-5p, and miR-205-5p levels in breastmilk sEVs from CUMS dams injected with AAV-MMTV-SP(miRNA) versus HC and CUMS dams injected with AAV-MMTV-SP(NC) (n = 7 mice per group). Data are presented as mean ± SEM. Statistical analysis was performed using one-way ANOVA followed by Bonferroni's multiple comparisons test (**e** and **f**), or two-sided unpaired t-test (**d**). **p < 0.01; ***p < 0.001.

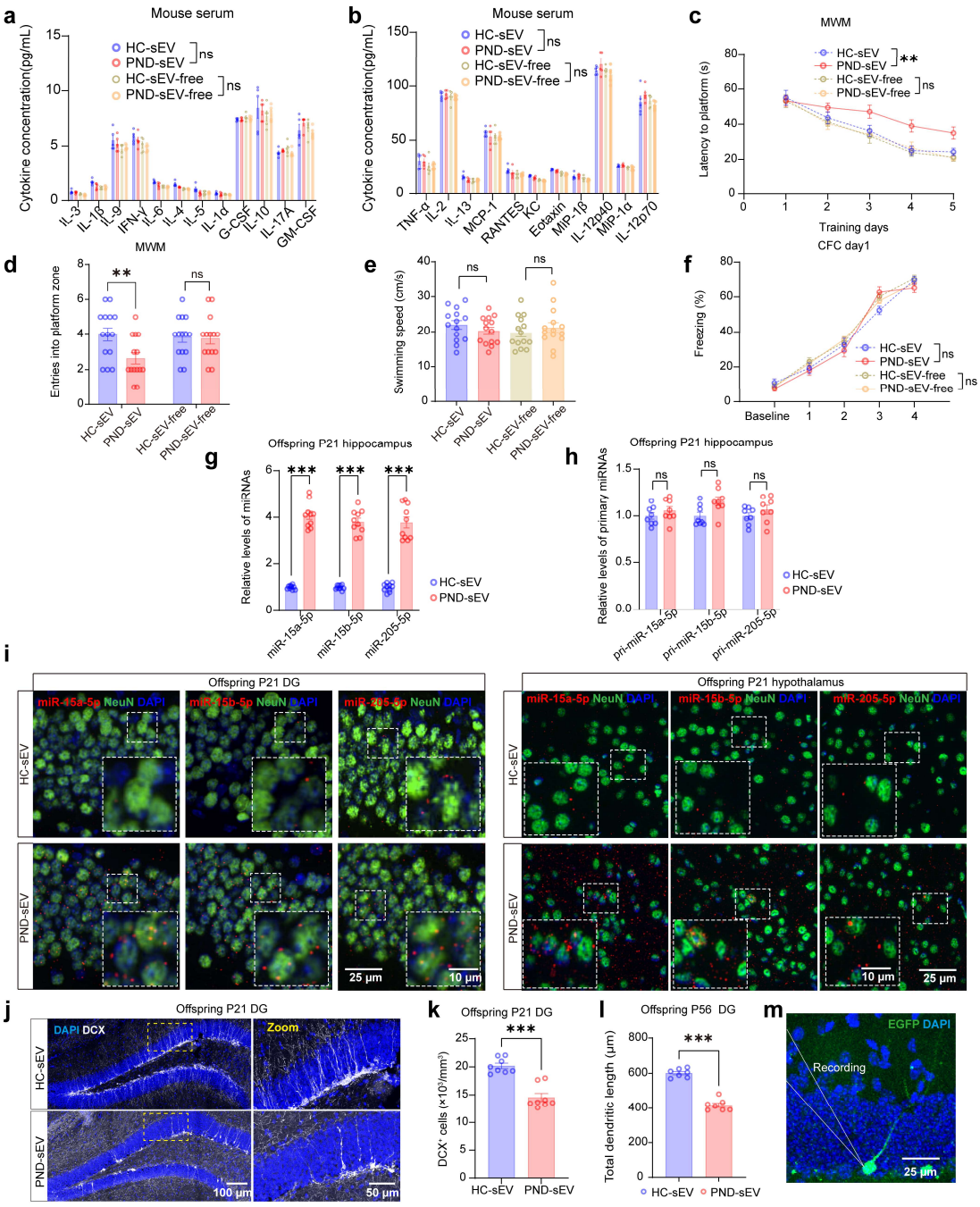

Supplementary Figure 11. Delivery of breastmilk sEVs and their miRNA cargo to the offspring hippocampus. a-b, Quantification of serum immune factors in pups treated with sEVs (HC-sEVs or PND-sEVs) or sEV-free fractions (HC-sEV-free or PND-sEV-free) isolated from the breastmilk of PND patients and HC mothers, analyzed by a Luminex liquid-phase chip assay (n = 5 per group). **c,** Latency to locate the hidden platform in the training trial of the MWM test (n = 18 for HC-sEV; n = 23 for PND-sEV). **d,** Number of entries into the platform zone in the probe trial of the MWM test (n = 14 per group). **e,** Total swimming activity in the MWM test (n = 14 for XXX). **f,** Freezing percentage in the training phase of the CFC test (n = 18 for HC-sEV; n = 23 for PND-sEV). **g,** Quantitative RT-PCR analysis of miR-15a-5p, miR-15b-5p, and miR-205-5p levels in the hippocampus of pups treated with HC-sEVs or PND-sEVs (n = 10 per group). **h,** Quantitative RT-PCR analysis of pri-miR-15a-5p, pri-miR-15b-5p, and pri-miR-205-5p levels in the hippocampus

of pups treated with HC-sEVs or PND-sEVs (n = 8 per group). **i,** RNAscope *in situ* hybridization of miR-15a-5p, miR-15b-5p, and miR-205-5p, combined with NeuN immunostaining, to visualize the distribution of these miRNAs in the hippocampal DG of pups treated with HC-sEVs or PND-sEVs. Representative images show positive miRNA dots (red) co-stained with NeuN (green) in the DG. Scale bars: 25 μm (overview), 10 μm (zoom). **j,** Left: Representative images of DCX staining in the DG of pups treated with HC-sEVs or PND-sEVs. Scale bars: 100 μm. Right: Magnified views of boxed areas, highlighting DCX^+ cell morphology and density. Scale bars: 50 μm. **k,** Quantification of DCX^+ cells in the DG of pups treated with HC-sEVs or PND-sEVs (n = 8 mice per group). **l,** Quantification of dendritic length in $EGFP^+$ newborn neurons from pups treated with HC-sEVs or PND-sEVs (n = 7 mice per group, averaging 17–20 cells per mouse). **m,** Representative images of recorded newborn neurons, identified and confirmed by $EGFP^+$ immunostaining signals (green) following RV-EGFP injection. Scale bars: 25 μm. Data are presented as mean ± SEM. Statistical analysis was performed using one-way ANOVA followed by Bonferroni's multiple comparisons test (**a, b,** and **e**), two-way ANOVA followed by Bonferroni's multiple comparisons test (**c** and **f**), or two-sided unpaired t-test (**d, g, h, k** and **l**). $^{**}p < 0.01$; $^{***}p < 0.001$; ns, not significant.

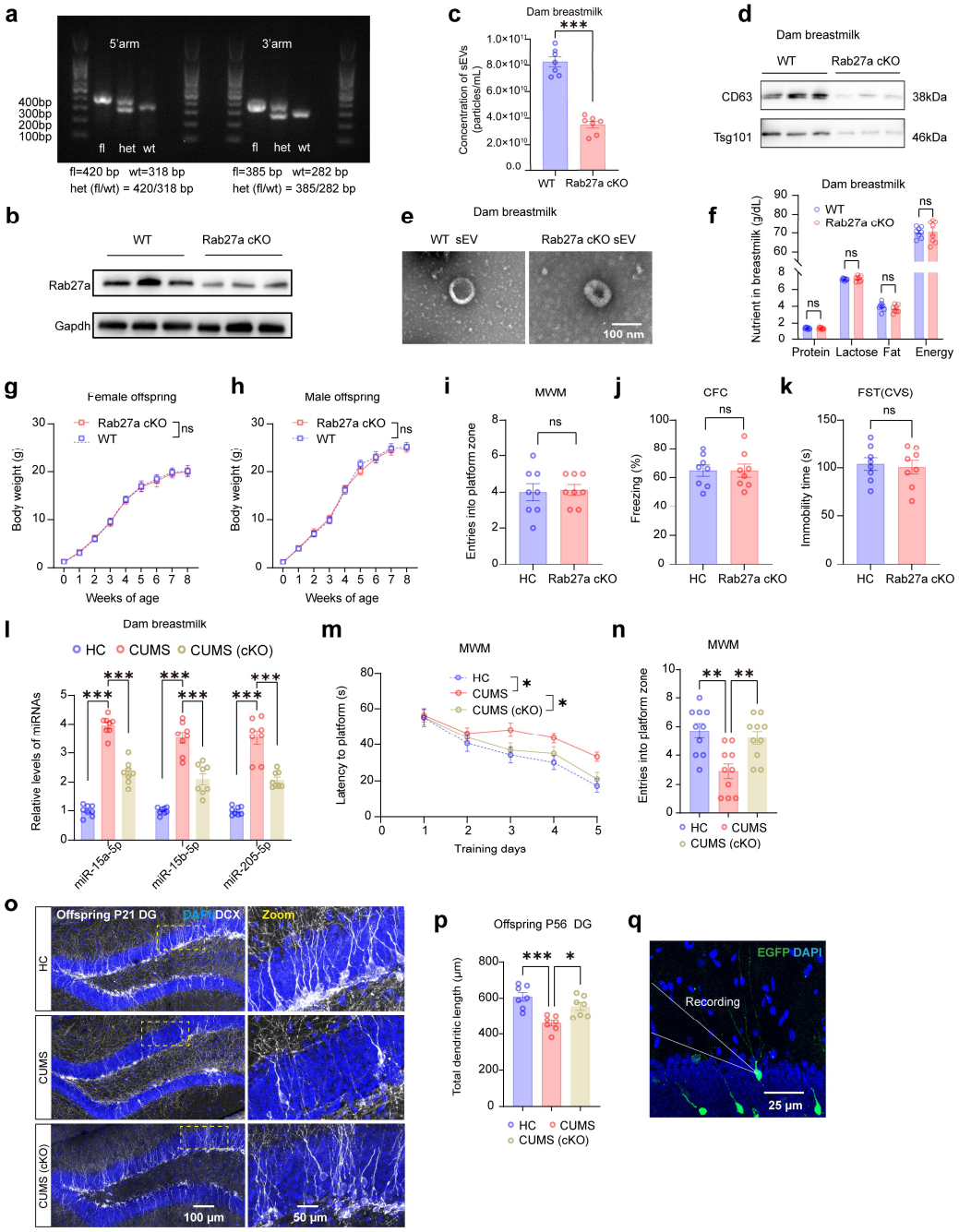

Supplementary Figure 12. Characterization of breastmilk sEVs from Rab27a cKO dams and their impact on offspring. Rab27a cKO dams were generated by injecting AAV2/9-MMTV-EGFP-IRES-Cre into the mammary glands of C57BL/6JGpt-Rab27a^{em1Cflox}/Gpt females. Wild-type (WT) and cKO dams were subjected to CUMS to induce a depression-like phenotype (CUMS (cKO) versus CUMS), and their fostered normal pups were monitored for phenotypic changes. Pups fostered by HC dams served as healthy controls. **a,** Genotype identification of Rab27a cKO mice by agarose gel electrophoresis. **b,** Western blot analysis of Rab27a protein in mammary tissues from WT and Rab27a cKO dams. **c,** Concentration of sEVs from the breastmilk of WT and Rab27a cKO dams (n = 7 per group). **d,** Western blot analysis of sEV markers (Tsg101 and CD63) in breastmilk sEVs from WT and Rab27a cKO dams. sEVs were isolated from an equivalent volume of breastmilk. **e,** Representative TEM images of breastmilk sEVs from WT and Rab27a cKO dams. Scale bars:

100 nm. **f,** Assessment of basic nutritional components (protein, carbohydrates, and fats) and total energy in breastmilk from WT and Rab27a cKO dams (n = 8 per group). **g-h,** Body weight changes in female **(g)** and male **(h)** offspring (n = 12 for female, n = 10 for male). **i,** Number of entries into the platform zone in the probe trial of the MWM test (n = 8 per group). **j,** Freezing percentage in the conditioning session of the CFC test (n = 8 per group). **k,** Immobility time in the FST after exposure to CVS (n = 8 per group). **l,** Quantitative RT-PCR analysis of miR-15a-5p, miR-15b-5p, and miR-205-5p levels in breastmilk from HC, CUMS, and CUMS (cKO) groups (n = 8 per group). **m,** Latency to locate the hidden platform in the training trial of the MWM test (n = 10 per group). **n,** Number of entries into the platform zone in the probe trial of the MWM test (n = 10 per group). **o,** Left: Representative images of DCX staining in the DG of pups. Scale bars: 100 μm. Right: Magnified views of boxed areas, highlighting DCX^+ cell morphology and density. Scale bars: 50 μm. **p,** Quantification of dendritic length in $EGFP^+$ newborn neurons (n = 7 mice per group). **q,** Representative images of recorded newborn neurons, identified and confirmed by $EGFP^+$ immunostaining signals (green) following RV-EGFP injection. Scale bars: 25 μm. Data are presented as mean ± SEM. Statistical analysis was performed using one-way ANOVA followed by Bonferroni's multiple comparisons test (**l, n,** and **p**), two-way ANOVA followed by Bonferroni's multiple comparisons test (**g, h,** and **m**), or two-sided unpaired t-test (**c, f, i, j,** and **k**). *$p < 0.05$; **$p < 0.01$; ***$p < 0.001$; ns, not significant.

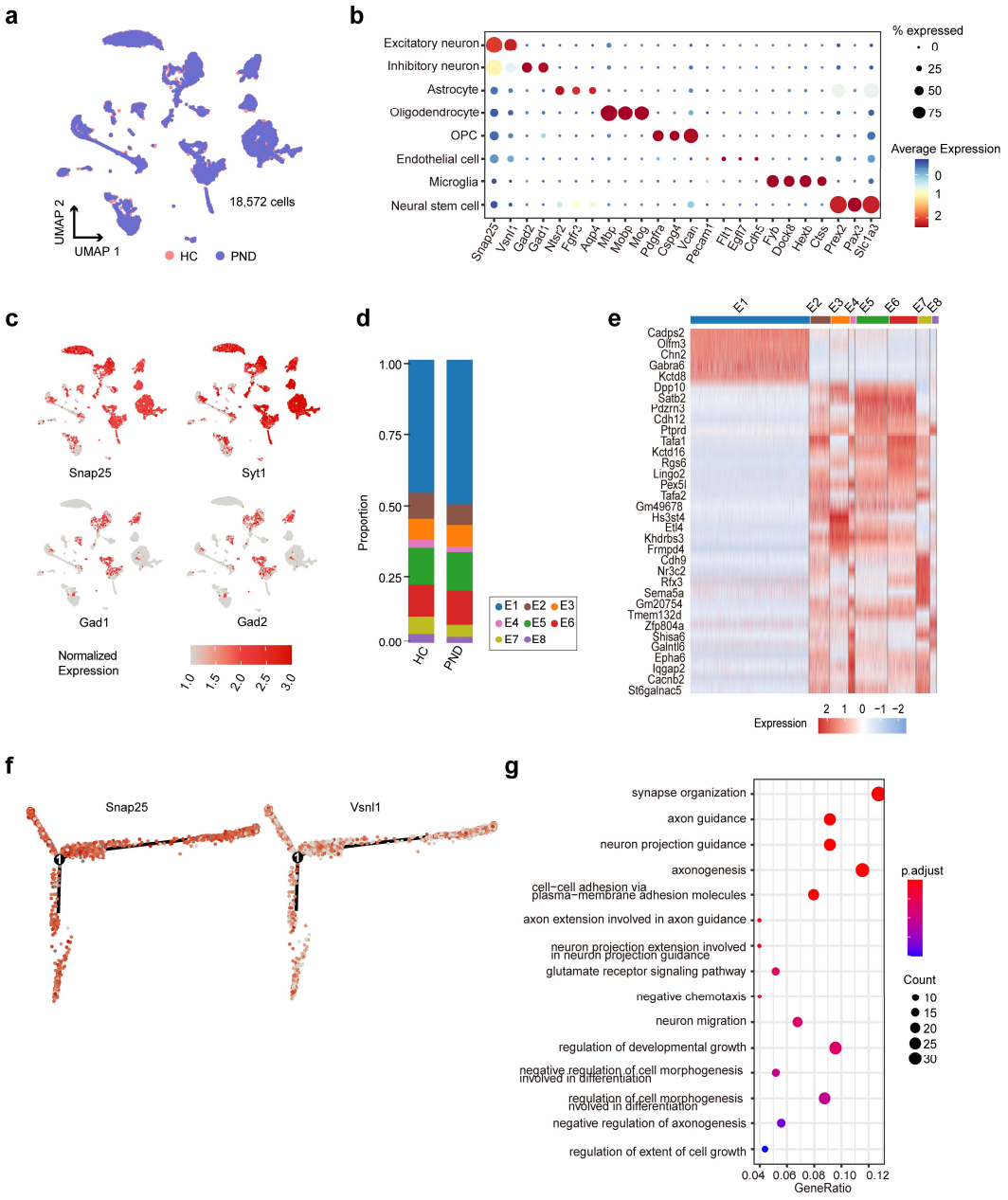

Supplementary Figure 13. Characterization of the E1 subpopulation of excitatory neurons in the DG. a, UMAP plot of 18,572 cells colored by samples. **b,** Dot plot showing representative marker genes across cell types. Dot size represents the proportion of expressing cells, and color intensity indicates the average expression level. **c,** Expression scatterplots of excitatory (top) and inhibitory (bottom) neuronal markers in different cell populations. **d,** Bar plot showing the percentage of different excitatory neuron subsets (E1–E8) in pups treated with HC-sEVs or PND-sEVs. **e,** Heatmap depicting the expression patterns of marker genes defining the eight subtypes of excitatory neurons. **f,** Pseudotime trajectories of excitatory neuron subtypes were inferred using Monocle2 and visualized by coloring them according to Snap25 and Syt1 gene expression. **g,** GO analysis of the 256 genes that are potential targets of miR-15a-5p, miR-15b-5p, and miR-205-5p. The top 15 significantly enriched biological processes are displayed based on adjusted p-values.

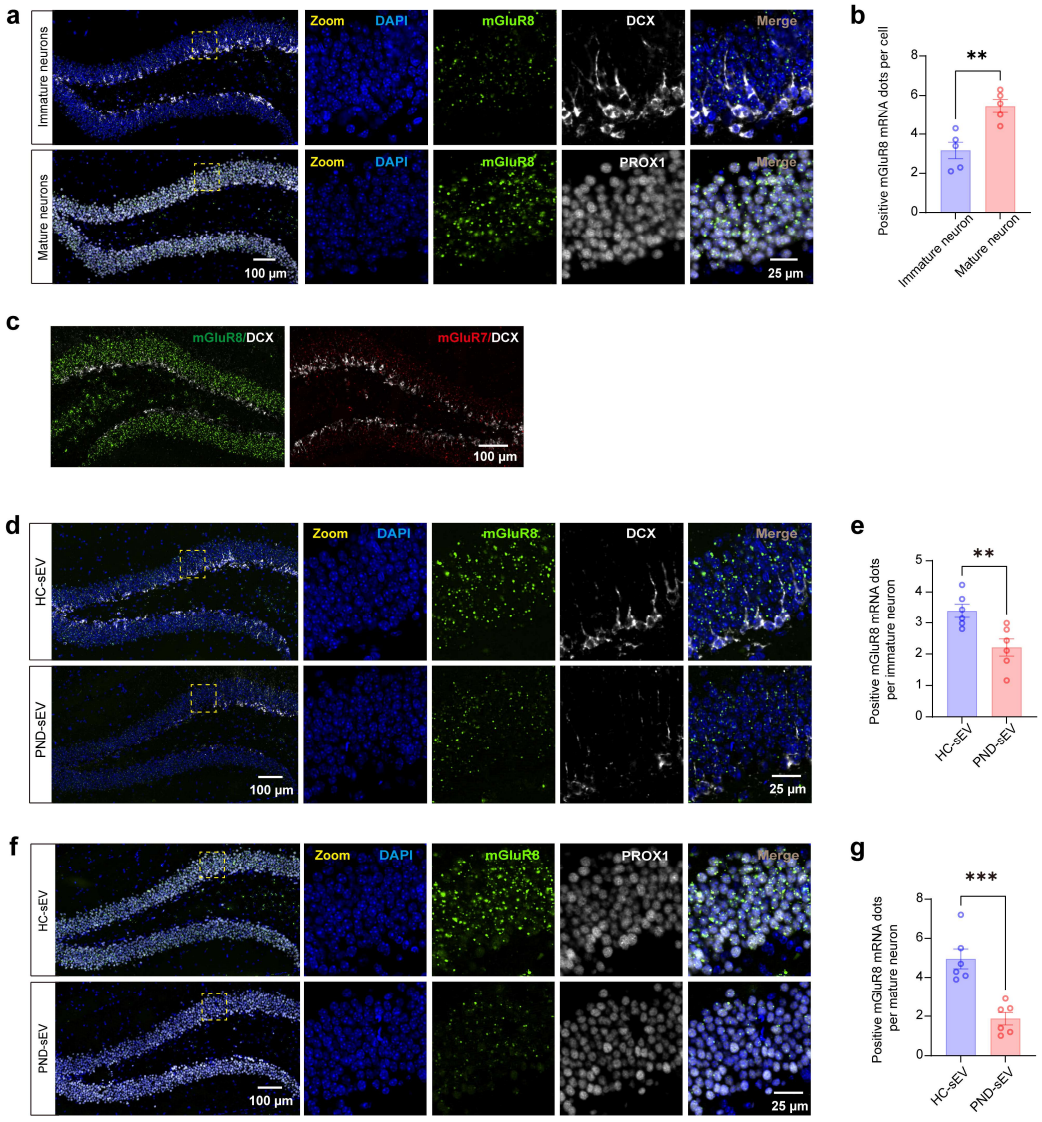

Supplementary Figure 14. Expression patterns of mGluR8 in the hippocampal DG of pups treated with HC-sEVs or PND-sEVs. a, RNAscope in situ hybridization of mGluR8, combined with immunostaining of DCX (top) or PROX1 (bottom), to visualize the distribution of mGluR8 in the hippocampal DG of pups under normal conditions. Left: Representative images showing mGluR8 mRNA hybridization signals colocalized with DCX$^+$ or PROX1$^+$ immunostaining in the DG. Scale bars: 100 μm. Right: Magnified views of boxed areas, highlighting colocalization of mGluR8 mRNA with DCX$^+$ or PROX1$^+$ cells in the DG. Scale bars: 25 μm. **b,** Quantification of positive dots of mGluR8 mRNA per DCX$^+$ or PROX1$^+$ cell (n = 5 mice per group, averaging 45 cells per mouse). **c,** RNAscope in situ hybridization of mGluR8 and mGluR7, combined with immunostaining of DCX, to visualize the distribution of mGluR8 and mGluR7 in the hippocampal DG of pups under normal conditions. Scale bars: 100 μm. **d,f,** RNAscope in situ hybridization of mGluR8, combined with immunostaining of DCX or PROX1, to visualize the distribution of mGluR8 in the hippocampal DG of pups treated with HC-sEVs or PND-sEVs. Left: Representative images showing mGluR8 mRNA hybridization signals colocalized with DCX$^+$ or PROX1$^+$ immunostaining in the DG. Scale bars: 100 μm. Right: Magnified views of boxed areas, highlighting

colocalization of mGluR8 mRNA with DCX^+ or $PROX1^+$ cells in the DG. Scale bars: 25 μm. **e,g,** Quantification of positive dots of mGluR8 mRNA per DCX^+ or $PROX1^+$ cell (n = 6 mice per group, averaging 45 cells per mouse). Data are presented as mean ± SEM. Statistical analysis was performed using two-sided unpaired t-test (**b, e,** and **g**). **$p < 0.01$; ***$p < 0.001$.

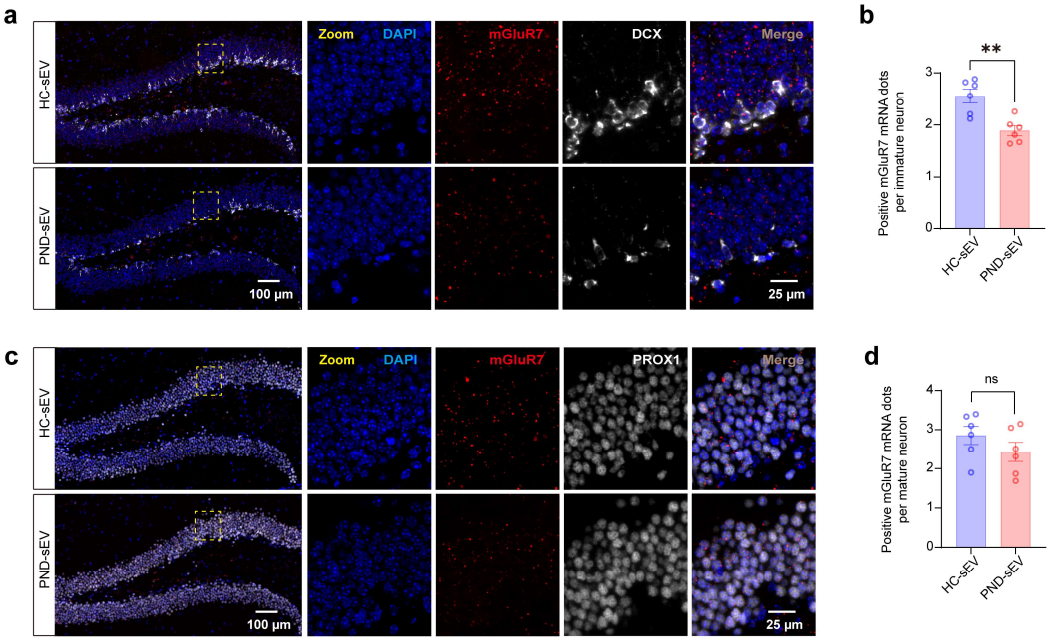

Supplementary Figure 15. Expression patterns of mGluR7 in the hippocampal DG of pups treated with HC-sEVs or PND-sEVs. a and **c,** RNAscope in situ hybridization of mGluR7, combined with immunostaining of DCX or PROX1, to visualize the distribution of mGluR7 in the hippocampal DG of pups treated with HC-sEVs or PND-sEVs. Left: Representative images showing mGluR7 mRNA hybridization signals colocalized with DCX^+ or $PROX1^+$ immunostaining in the DG. Scale bars: 100 μm. Right: Magnified views of boxed areas, highlighting colocalization of mGluR7 mRNA with DCX^+ or $PROX1^+$ cells in the DG. Scale bars: 25 μm. **b** and **d,** Quantification of positive dots of mGluR7 mRNA per DCX^+ or $PROX1^+$ cell (n = 6 mice per group, averaging 45 cells per mouse). Data are presented as mean ± SEM. Statistical analysis was performed using two-sided unpaired t-test (**b** and **d**). **$p < 0.01$; ns, not significant.

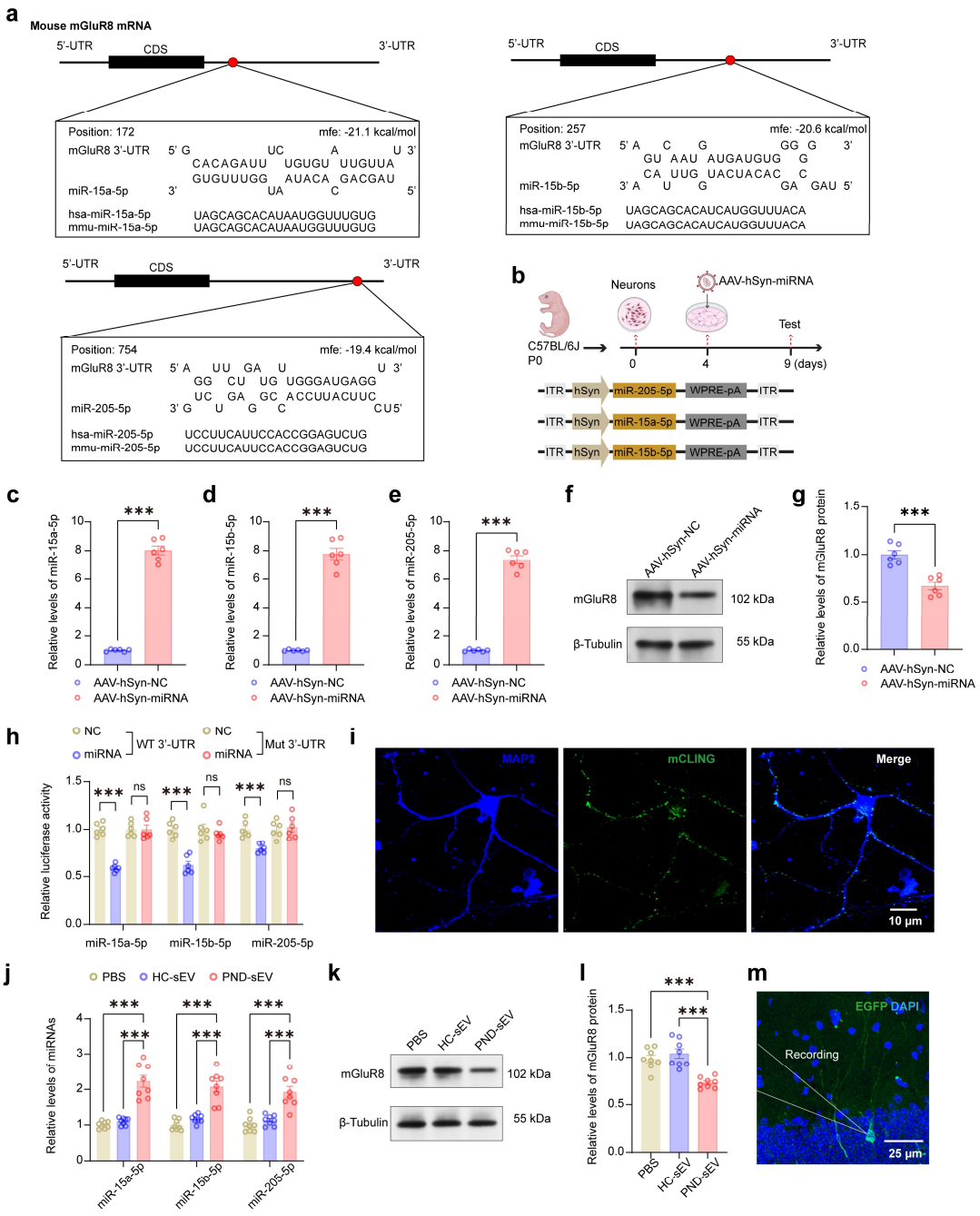

Supplementary Figure 16. ***In vitro*** **validation of mGluR8 regulation by miR-15a-5p, miR-15b-5p, and miR-205-5p, and its functional impact on neuronal development and synaptic plasticity. a,** Schematic of the predicted binding sites for miR-15a-5p, miR-15b-5p, and miR-205-5p within the 3'-UTR of mGluR8 mRNA, with the minimum free energy of each hybrid indicated. **b,** Experimental scheme for AAV-mediated overexpression of miR-15a-5p, miR-15b-5p, and miR-205-5p in cultured primary neurons. Neurons from wild-type mice were transfected with a pool of three AAVs (AAV-hSyn-miRNA) or a negative control AAV (AAV-hSyn-NC). mGluR8 knockdown efficiency was evaluated three days post-infection. **c-e,** Quantitative RT-PCR analysis of miR-15a-5p, miR-15b-5p, and miR-205-5p levels in neurons transfected with AAV-hSyn-miRNA or AAV-hSyn-NC (n = 6 per group). **f,g,** Western blot analysis of mGluR8 protein levels in hippocampal neurons transfected with AAV-hSyn-miRNA or AAV-hSyn-NC. Representative Western blot images

and densitometric analysis of mGluR8 band density normalized to β-Tubulin (n = 6 per group) are shown. **h,** Firefly luciferase reporters containing either wild-type (WT) or mutant (Mut) miRNA binding sites in the 3'-UTR of mGluR8 were co-transfected into HEK293T cells along with synthetic miRNAs or synthetic negative control RNA (NC). Twenty-four hours post-transfection, HEK293T cells were analyzed using a luciferase assay kit. A reduction in luciferase activity observed only in the WT reporters indicates direct binding of the corresponding miRNAs to the predicted sites in the 3'-UTR of mGluR8 (n = 6 per group). **i,** Z-merged 3D confocal images showing mCLING-labeled sEVs within MAP2-labeled neurons, with most mCLING signals appearing as punctate labels around the nucleus. Scale bars: 10 μm. **j,** Quantitative RT-PCR analysis of miR-15a-5p, miR-15b-5p, and miR-205-5p levels in neurons treated with HC-sEVs or PND-sEVs. **k-l,** Western blot analysis of mGluR8 protein levels in neurons treated with PBS, HC-sEVs, or PND-sEVs. Representative Western blot images and densitometric analysis of mGluR8 band density normalized to β-Tubulin (n = 8 per group) are shown. **m,** Representative images of recorded newborn neurons, identified and confirmed by $EGFP^+$ immunostaining signals (green) following RV-EGFP injection. Scale bars: 25 μm. Data are presented as mean ± SEM. Statistical analysis was performed using one-way ANOVA followed by Bonferroni's multiple comparisons test (**h, j** and **l**), or two-sided unpaired t-test (**c-e** and **g**). **$p < 0.01$; ***$p < 0.001$; ns, not significant.

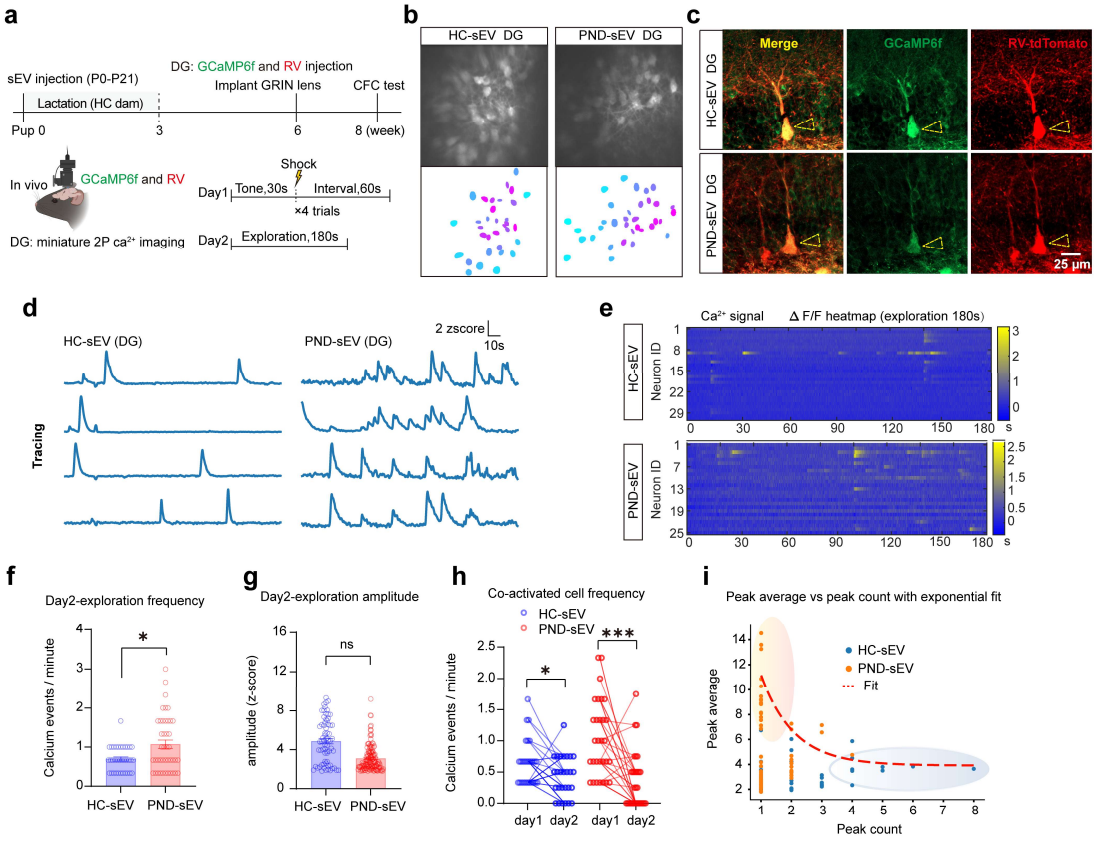

Supplementary Figure 17. *In vivo* calcium imaging reveals a "high-frequency, low-amplitude" activation profile in DG neurons after PND-sEV administration. a, Schematic of the experimental workflow to assess the impact of PND-sEVs on SuM→DG projections. Normal pups received daily intragastric administration of equal amounts of PND-sEVs or HC-sEVs throughout lactation. A genetically encoded calcium indicator (GCaMP6f) and RV-tdTomato were co-injected into the DG for calcium imaging. Miniature two-photon calcium imaging was used to record DG neuronal activity during a CFC paradigm. On Day 1, mice underwent 4 trials of tone stimulation (30 s) paired with a foot shock, with 60 s inter-trial intervals. On Day 2, neuronal activity was recorded during a 180 s exploration period in the same context without stimulation. **b,** Representative average time-series calcium images of the DG. **c,** Representative fluorescence images of the DG. GCaMP6f fluorescence signal (green) indicates labeled DG neurons; merged images show co-localization of viral labels. Scale bars: 25 μm. **d,** Example calcium traces of DG neurons. **e,** Calcium activity heatmaps of DG neurons during the 180 s exploration phase on Day 2. Each row represents the calcium dynamics of a single neuron (labeled by Neuron ID). **f-g,** Calcium event frequency (F) and amplitude (G) in DG neurons during the exploration phase on Day 2. **h,** Calcium event frequency in context-related DG neurons (activated during the interval phase on Day 1). **i,** Frequency-amplitude distribution of calcium events, fitted with an exponential model. Each point represents the amplitude of a calcium event at a given frequency. Dashed lines indicate the exponential fit. n = 3 mice per group for all figures. Data are presented as mean ± SEM. Statistical analysis was performed using two-way ANOVA followed by Bonferroni's multiple comparisons test (**h**), or two-sided unpaired t-test (**f** and **g**). *p < 0.05; ***p < 0.001; ns, not significant.

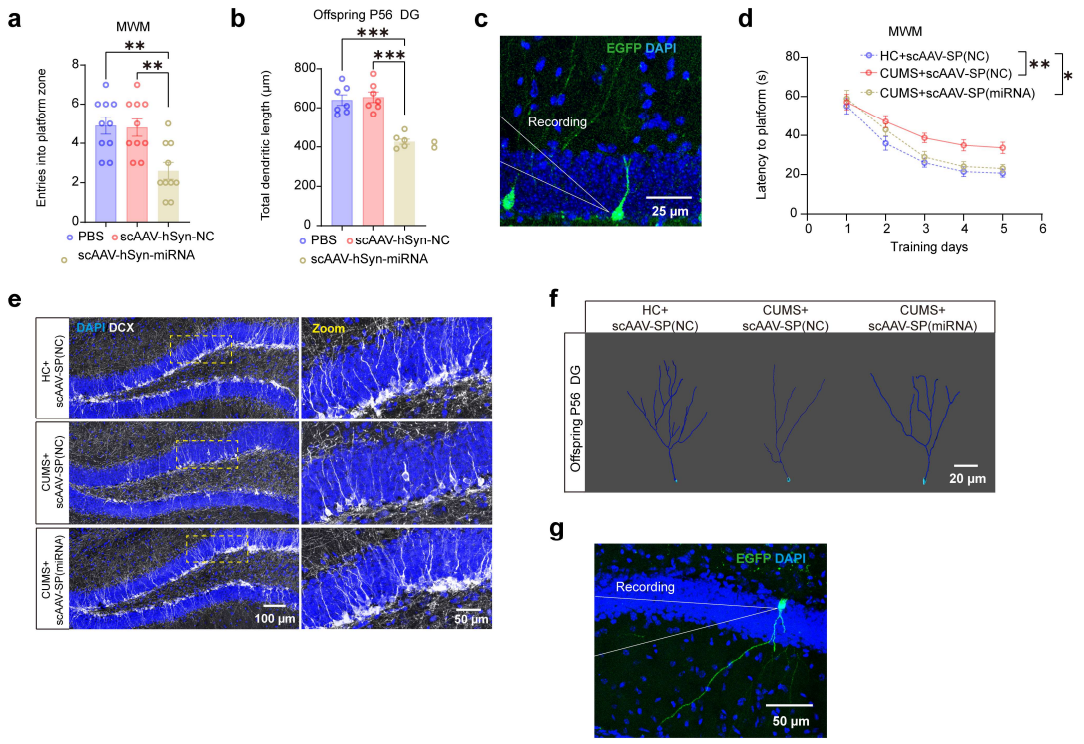

Supplementary Figure 18. Bidirectional manipulation of hippocampal miRNA activity influences offspring neurodevelopment. a, Number of entries into the platform zone in the probe trial of the MWM test for the PBS, scAAV-hSyn-NC, and scAAV-hSyn-miRNA groups (n = 10 mice per group). **b,** Quantification of dendritic length in EGFP$^+$ newborn neurons from the PBS, scAAV-hSyn-NC, and scAAV-hSyn-miRNA groups at P56 (n = 7 mice per group, 17-20 cells/mouse). **c,** Representative images of recorded newborn neurons, identified and confirmed by EGFP$^+$ immunostaining signals (green) following RV-EGFP injection. Scale bars: 25 μm. **d,** Latency to locate the hidden platform in the training trial of the MWM test (n = 12 per group) **e,** Left: Representative images of DCX staining in the DG from the HC + scAAV-hSyn-SP(NC), CUMS + scAAV-hSyn-SP(NC), and CUMS + scAAV-hSyn-SP(miRNA) groups. Scale bar: 100 μm. Right: Magnified views of boxed areas, highlighting DCX$^+$ cell morphology and density. Scale bars: 50 μm. **f,** Representative images showing the dendritic morphology of EGFP$^+$ newborn neurons in the HC + scAAV-hSyn-SP(NC), CUMS + scAAV-hSyn-SP(NC), and CUMS + scAAV-hSyn-SP(miRNA) groups at P56. Scale bars: 20 μm. **g,** Representative images of recorded newborn neurons, identified and confirmed by EGFP$^+$ immunostaining signals (green) following RV-EGFP injection. Scale bars: 50 μm. Data are presented as mean ± SEM. Statistical analysis was performed using one-way ANOVA followed by Bonferroni's multiple comparisons test (**a** and **b**), or two-way ANOVA followed by Bonferroni's multiple comparisons test (**d**). **p < 0.01; ***p < 0.001.

Supplementary Table 1. Key resources table.

REAGENT or RESOURCE	SOURCE	IDENTIFIER
Antibodies		
rabbit anti-c-Fos	Abcam	Cat# ab214672, RRID: AB_2939046
mCLING-ATTO 488-labeled	Synaptic Systems	Cat# 710 006AT3, NA
mouse anti-BrdU	Millipore	Cat# MAB4072, RRID: AB_95024
rat anti-BrdU	Abcam	Cat# ab6326, RRID: AB_305426
mouse anti-Nestin	Millipore	Cat# MAB353, RRID: AB_94911
rabbit anti-PCNA	Cell Signaling Technology	Cat# 13110, RRID: AB_2636979
mouse anti-Mcm2	BD Biosciences	Cat# 610700, RRID: AB_2141952
rabbit anti-DCX	Cell Signaling Technology	Cat# 91954, RRID: AB_561007
rabbit anti-NeuN	Cell Signaling Technology	Cat# 24307, RRID:AB_2651140
mouse anti-β-tubulin	Yeasen	Cat# 30302ES20, NA
mouse anti-α-tubulin	Proteintech	Cat# 11224-1-AP, RRID: AB_2210206
rabbit anti-mGluR8	Abcam	Cat# ab53094, RRID: AB_881224
rabbit anti-PROX1	Abcam	Cat# ab199359, RRID: AB_2868427
mouse anti-MAP2	Abcam	Cat# ab11267, RRID: AB_297885
mouse anti-PSD95	Abcam	Cat# ab2723, RRID: AB_303248
rabbit anti-Synapsin I	Millipore	Cat# AB1543, RRID: AB_2200400
rabbit anti-TSG101	Abcam	Cat# ab125011, RRID: AB_10974262
rabbit anti-CD63	Abcam	Cat# ab217345, RRID: AB_2754982
rabbit anti-LTF	ABclonal	Cat#A12902, RRID: AB_2759747
rabbit anti-Rab27A	Cell Signaling Technology	Cat# 69295, RRID：AB_2799759
Goat-anti-Mouse IgG-HRP	Santa Cruz	Cat# sc-2031; RRID: AB_631737
Goat anti-Rabbit IgG-HRP	Cell Signaling Technology	Cat# 7074S; RRID: AB_2099233

Anti-Rabbit IgG, Alexa Fluor 488	Thermo Fisher Scientific	Cat# A-11034, RRID: AB_2576217
Anti-Mouse IgG, Alexa Fluor 488	Thermo Fisher Scientific	Cat# R37120, RRID: AB_2556548
Anti-Mouse IgG, Alexa Fluor 594	Thermo Fisher Scientific	Cat# R37121, RRID: AB_2556549
Anti-Rabbit IgG, Alexa Fluor 594	Thermo Fisher Scientific	Cat# R37117, RRID: AB_2556545
anti-Rabbit IgG, Alexa Fluor 647	Thermo Fisher Scientific	Cat# A-31573, RRID: AB_2536183
anti-Rat IgG, Alexa Fluor 594	Thermo Fisher Scientific	Cat# A-21209, RRID: AB_2535795
Virus strains		
rAAV-miR-302f 3'UTR-mCherry-WPREs	Taitool Bioscience	Cat# WY4640
rAAV-mCherry- hsa_miR-302f -WPREs	Taitool Bioscience	Cat# WY4641
VSVG-Retrovirus-esEF1a-EGFP-WPRE-pA VSVG-R5004	Taitool Bioscience	Cat# VSVG-R5004
AAV2/9-hSyn-mmu-miR-15b-EGFP-WPRE-PA	Taitool Bioscience	Cat# WY4524
AAV2/9-hSyn-mmu-miR-15a-EGFP-WPRE-pA	Taitool Bioscience	Cat# WY4523
AAV2/9-hSyn-mmu-miR-205-EGFP-WPRE-pA	Taitool Bioscience	Cat# WY4525
scAAV2/9-hSyn-mCherry-Sponge (miR-15b-5p)W3SLpA	Taitool Bioscience	Cat# WY4527
scAAV2/9-hSyn-EGFP-Sponge (miR-205-5p) W3SLpA	Taitool Bioscience	Cat# WY4528
scAAV2/9-hSyn-EBFP-Sponge (miR-15a-5p) W3SLpA	Taitool Bioscience	Cat# WY4526
scAAV2/9-hSyn-EGFP-WPRE-pA	Taitool Bioscience	Cat# S0581-9-H20
scAAV2/9-hSyn-EBFP-WPRE-pA	Taitool Bioscience	Cat# S1381-9-H50
scAAV2/9-hSyn-mCherry-WPRE-pA	Taitool Bioscience	Cat# S1382-9-H50
AAV2/9-hSyn-EGFP-3xFlag-WPRE-pA	Taitool Bioscience	Cat# S0237-9-H50
AAV2/9-hSyn-DIO-mGFP-WPRE-pA	Taitool Bioscience	Cat# S0276-9
AAV2/9-hSyn-Cre-WPRE-pA	Taitool Bioscience	Cat# S0278-9
rAAV-hSyn-GCAMP6f-WPRE-hGH pA	BrainVTA	N/A
AAV2/9-hSyn-DIO-GRM8-mCherry-pA	Taitool Bioscience	Cat# WY5268

AAV2/9-hSyn-DIO-MasterRNAi155(GRM8)-mCherry-WPRE-pA	Taitool Bioscience	Cat# WY5269
AAV2/9-hSyn-DIO-MasterRNAi155(NC)-mCherry-WPRE-pA	Taitool Bioscience	Cat# S0769-9
AAV2/9-hSyn-DIO-mCherry-pA	Taitool Bioscience	Cat# S0240-9
AAV2/2Retro Plus-hSyn-Cre-EGFP-WPRE-pA	Taitool Bioscience	Cat# S0230-2RP
AAV2/9-MMTV-EGFP-IRES-Cre-W3SLpA	Taitool Bioscience	Cat# WY5264
rAAV-hSyn-mCherry-WPRE-hGH polyA	BrainVTA	Cat# PT-0100
AAV2/9-MMTV-miR-15b-EGFP-WPRE-PA	Taitool Bioscience	Cat# WY4543
AAV2/9-MMTV-miR-15a-EGFP-WPRE-pA	Taitool Bioscience	Cat# WY4542
AAV2/9-MMTV-miR-205-EGFP-WPRE-pA	Taitool Bioscience	Cat# WY4544
AAV2/9-MMTV-mCherry-Sponge (miR-15b-5p)W3SLpA	Taitool Bioscience	Cat# WY4529
AAV2/9-MMTV-mCherry-Sponge (miR-205-5p) W3SLpA	Taitool Bioscience	Cat# WY4530
AAV2/9-MMTV-mCherry-Sponge (miR-15a-5p) W3SLpA	Taitool Bioscience	Cat# WY4531
Chemicals, peptides, and recombinant proteins		
BrdU	Sigma-Aldrich	Cat# B5002
DAPI	Invitrogen	Cat# D1306
TRIzol	Invitrogen	Cat#15596018
Neurobasal medium	Thermo Fisher Scientific	Cat# 21103–049
B27 supplement	Thermo Fisher Scientific	Cat# 17504–044
GlutaMax	Thermo Fisher Scientific	Cat# 35050–061
poly-D-lysine	Sigma-Aldrich	Cat# P0899
Lipofectamine RNAiMAX reagent	ThermoFisher Scientific	Cat# 13778-075
Triton X-100	Roche	Cat# 11332481001
DMEM/F-12	Gibco	Cat# 11320082

RIPA buffer	Yeasen	Cat# 20101ES60
Collagenase D	Sigma-Aldrich	Cat# 11088866001
Econo-Pac column	BioRad	Cat# 7321010
Bestarose CL-6B resin	Bestchrom	Cat# AG0044
Critical commercial assays		
ECL Western Blotting Substrate	Thermo Fisher Scientific	Cat# 32106
Single Cell-to-CT qRT-PCR	Thermo Fisher Scientific	Cat# 4458237
miRNAscope HD Reagent Kit-RED	Advanced Cell Diagnostics	Cat# 324500
RNAscope Multiplex Fluorescent Reagent Kit v2	Advanced Cell Diagnostics	Cat# 323100
TaqMan microRNA cDNA Synthesis Kit	Thermo Fisher Scientific	Cat# 4366597
TaqMan Universal Master Mix II, no UNG	Thermo Fisher Scientific	Cat# 4440038
Oligonucleotides		
TaqMan MicroRNA Assay Probe	Thermo Fisher Scientific	Cat# 4427975
miRNAscope Probe-SR-miR-15b-5p-S1	Advanced Cell Diagnostics	Cat# 1109211-S1
miRNAscope Probe-SR-miR-15a-5p-S1	Advanced Cell Diagnostics	Cat# 1218691-S1
miRNAscope Probe-SR-miR-205-5p-S1	Advanced Cell Diagnostics	Cat# 728541-S1
RNAscope Probe-Mm-Grm7	Advanced Cell Diagnostics	Cat# 487841
RNAscope Probe-Mm-Grm8-C2	Advanced Cell Diagnostics	Cat# 521491-C2
GAPDH RT-PCR primer forward	GenScript	Seq: 5’-AGGTCGGTGTGAACGGATTTG-3’
GAPDH RT-PCR primer reverse	GenScript	Seq: 5’-TGTAGACCATGTAGTTGAGGTC-3’
mGluR8 RT-PCR primer forward	GenScript	Seq: 5’-CAGCACTCACGGTCAGAGT-3’
mGluR8 RT-PCR primer reverse	GenScript	Seq: 5’-TGAATTCAGCCCTGTAGCAGA-3’
miRNA mimics	GenScript	N/A
Recombinant DNA		

mGluR8-luc-WT_pMIR-REPORT Luciferase	GenScript	N/A
mGluR8-luc-Mutant_pMIR-REPORT Luciferase	GenScript	N/A
Cell line		
HEK293 cell line	ATCC	CRL-11268
Experimental models: Organisms/strains		
Mouse: C57BL/6J	Nanjing Biomedical Research Institute of Nanjing University (NBRI)	N/A
Mouse: Rosa26-CD63^{Flag}EGFP	NBRI	N/A
Mouse: CD-1	NBRI	N/A
Mouse: B6-CAG-Cre	NBRI	N/A
Deposited data		
RNA sequence raw data	National Genomics Data Center (China National Center for Bioinformaton)	PRJCA035478, PRJCA036054
Software and algorithms		
GraphPad Prism 8	Graphpad	RRID: SCR_002798
Image J	Image J	RRID:SCR_003070
SPSS software (version 20.0)	IBM	RRID:SCR_01909
Bio-Rad Chemidoc XRS Gel Imaging	Bio-Rad	RRID:SCR_019690
LightCycler®96 Version 1.1.0.1320	Roche	N/A

Supplementary Table 2. Demographics, depression scale, and serum biochemical indicators in HC mothers and PND patients.

Variable	HC Mothers (Mean ± SEM)	PND Patients (Mean ± SEM)	P-value
Sample Size (n)	40	51	
EPDS Score	3.21 ± 0.29	15.24 ± 0.54	<0.001*
Age (years)	30.84 ± 0.79	30.37 ± 0.70	0.656
Gestational age at delivery (weeks)	38.38 ± 0.38	38.50 ± 0.33	0.805
Number of previous births	0	0	/
Pre-pregnancy BMI (kg/m^2)	28.26 ± 0.78	27.20 ± 0.47	0.230
FPG (mmol/L)	4.39 ± 0.07	4.52 ± 0.06	0.182
HbA1c (%)	4.99 ± 0.05	5.08 ± 0.06	0.294
Total protein (g/L)	64.21 ± 0.94	64.72 ± 0.72	0.664
Albumin (g/L)	35.64 ± 0.40	36.34 ± 0.41	0.250
TAG (mmol/L)	3.01 ± 0.20	2.88 ± 0.23	0.677
LDL cholesterol (mmol/L)	3.62 ± 0.19	3.47 ± 0.14	0.500
HDL cholesterol (mmol/L)	2.25 ± 0.07	2.10 ± 0.06	0.111

Calcium (mmol/L)	2.16 ± 0.02	2.18 ± 0.02	0.555

Data are mean ± standard deviation. Statistical analysis was performed using two-sided unpaired t-test. *P<0.05 was considered significant.

Abbreviations: EPDS, Edinburgh Postnatal Depression Scale; BMI, body mass index; FPG, Fasting Plasma Glucose; TAG, Triglyceride; HbA1c, glycated hemoglobin; HDL, high-density lipoprotein; LDL, low-density lipoprotein.

Supplementary Table 3. Nutrient levels in breastmilk from HC mothers and PND patients.

Variable	HC Mothers (Mean ± SEM)	PND Mothers (Mean ± SEM)	P-value
Sample Size (n)	40	51	
Total protein (g/L)	1.35 ± 0.03	1.36 ± 0.03	0.816
Total Carbohydrate (g/L)	7.38 ± 0.11	7.34 ± 0.13	0.744
Total Fat (g/L)	3.82 ± 0.23	3.86 ± 0.30	0.811
Energy (kcal/L)	72.38 ± 1.84	73.91 ± 2.36	0.511

Data are mean ± standard deviation. Statistical analysis was performed using two-sided unpaired t-test.